EFFECT OF ATMOSPHERIC CONDITIONS ON COVERAGE OF FOGGER APPLICATIONS IN A DESERT SURFACE BOUNDARY LAYER

D. R. Miller, L. R. Khot, A. L. Hiscox, M. Salyani, T. W. Walker, M. Farooq

ABSTRACT. *Near-ground aerosol fogs were applied in the Chihuahua Desert of New Mexico, which has widely spaced, low shrub vegetation. Near-ground fog dispersion was measured remotely with a light detection and ranging (lidar) system. Local atmospheric turbulence and stability were continuously measured with 3-axis sonic anemometers during aerosol treatments. Lidar-measured plume area coverage and spread were related to the simultaneous local-scale weather, including both convective boundary layers (CBL) and stable boundary layers (SBL). A modified bulk stability ratio (SRm) was used to characterize the stability conditions near the ground. Time averages appropriate to the SBL were determined using the multidimensional decomposition technique and matched to the short spray time periods in the CBL. The widest, most effective, near-ground coverage was obtained from insect fogger applications conducted during relatively high wind speeds: $U > 1$ m s^{-1} in stable conditions, and $U > 3$ m s^{-1} in unstable conditions. In general, spraying during SBLs was more efficient than during CBLs, with less material wasted and better consistency of coverage in the target zone nearest the ground. There was no significant difference in spray coverage or plume dispersion between the handheld thermal fogger and the ultra-low volume (cold fogger) applicator used.*

Keywords. *Aerosol plume, Atmospheric stability, Droplet dispersion, Lidar, Sand flies.*

Leishmaniasis, a vector-borne disease caused by sand flies, is a persistent health threat to U.S. military personnel deployed to Iraq, Afghanistan, and other Middle East countries (Aronson, 2007; Pages et al., 2010). There are reports of over 1000 cases of Leishmaniasis among U.S. soldiers deployed in Iraq during 2003-2004 (Pages et al., 2010). About 23% of deployed U.S. ground forces during 2003-2005 were infected with Leishmaniasis (McFee, 2008). Techniques such as: use of residual insecticide sprays on tents, dusting fences and tree lines with carbaryl, and nighttime ultra-low volume (ULV) spray have been ineffective for sand flies control (Aronson, 2007). The ineffectiveness of these techniques is likely due to the nighttime activity and close-to-ground flying habits of sand flies (USACHPPM, 2005). To be effective, the spray droplets must stay suspended near the ground with maximum horizontal spread. Therefore, this project involved characterizing the aerosol coverage of ULV applicators and thermal foggers under different stability conditions, especially nighttime field conditions.

A key factor in the evaluation of field aerosol application involves using appropriate plume drift assessment techniques. Common field methods of plume drift measurement are complex, expensive, and inadequate for measuring plumes of drifting aerosols (Miller et al., 2003). The direct techniques of spray drift assessment involve using fixed passive and active air samplers during field experiments (Salyani and Cromwell, 1992; Barber et al., 2004; Bonds et al., 2009; Farooq et al., 2009; Schleier and Peterson, 2010). Basic spray dispersion has also been studied using indirect techniques such as phase Doppler particle analyzers (PDPA) and wind tunnel measurements (Nuyttens et al., 2009). Laboratory-based techniques do not include local atmospheric effects. Collins (1968), Hoff et al. (1989), Mickle (1994), Miller et al. (2003), Hiscox et al. (2006a), and Solanelles et al. (2009) have developed and used light detection and ranging (lidar) techniques to remotely evaluate spray plume dispersion in the field. The lidar techniques offer real-time mapping of remotely sensed spray drift with the additional capability of plume movement visualization. Lidar has been used successfully to observe spray dispersion in nighttime stable (Hiscox et al., 2006b) and daytime unstable atmospheric conditions (Stoughton et al., 1997; Stoughton and Miller, 2002). Lidar

Submitted for review in February 2011 as manuscript number PM 9067; approved for publication by the Power & Machinery Division of ASABE in January 2012.

The authors are **David R. Miller,** Professor Emeritus, Department of Natural Resources and the Environment, University of Connecticut, Storrs, Connecticut; **Lav R. Khot, ASABE Member,** Postdoctoral Research Associate, Department of Agricultural and Biological Engineering, Citrus Research and Education Center, University of Florida, Lake Alfred, Florida; **April L. Hiscox, ASABE Member,** Assistant Professor, Department of Geography, University of South Carolina, Columbia, South Carolina; **Masoud Salyani, ASABE Member,** Professor, Department of Agricultural and Biological Engineering, Citrus Research and Education Center, University of Florida, Lake Alfred, Florida; **Todd W. Walker,** Medical Entomologist, and **Muhammad Farooq, ASABE Member,** Agricultural Engineer, U.S. Navy Entomology Center of Excellence, Jacksonville, Florida. **Corresponding author:** Masoud Salyani, Department of Agricultural and Biological Engineering, Citrus Research and Education Center, University of Florida, Lake Alfred, FL 33850; phone: 863-956-1151, ext. 18711; fax: 863-956-4631; e-mail: msi@ufl.edu.

 © 2012 American Society of Agricultural and Biological Engineers ISSN 2151-0032

Report Documentation Page

Form Approved
OMB No. 0704-0188

Public reporting burden for the collection of information is estimated to average 1 hour per response, including the time for reviewing instructions, searching existing data sources, gathering and maintaining the data needed, and completing and reviewing the collection of information. Send comments regarding this burden estimate or any other aspect of this collection of information, including suggestions for reducing this burden, to Washington Headquarters Services, Directorate for Information Operations and Reports, 1215 Jefferson Davis Highway, Suite 1204, Arlington VA 22202-4302. Respondents should be aware that notwithstanding any other provision of law, no person shall be subject to a penalty for failing to comply with a collection of information if it does not display a currently valid OMB control number.

1. REPORT DATE	2. REPORT TYPE	3. DATES COVERED
2012		**00-00-2012 to 00-00-2012**

4. TITLE AND SUBTITLE	5a. CONTRACT NUMBER
Effect of Atmospheric Conditions on Coverage of Fogger Applications in a Desert Surface Boundary Layer	5b. GRANT NUMBER
	5c. PROGRAM ELEMENT NUMBER
6. AUTHOR(S)	5d. PROJECT NUMBER
	5e. TASK NUMBER
	5f. WORK UNIT NUMBER
7. PERFORMING ORGANIZATION NAME(S) AND ADDRESS(ES) **University of Florida,Department of Agricultural and Biological Engineering,Citris Research and Education Center,Lake Alfred,FL,33850**	8. PERFORMING ORGANIZATION REPORT NUMBER
9. SPONSORING/MONITORING AGENCY NAME(S) AND ADDRESS(ES)	10. SPONSOR/MONITOR'S ACRONYM(S)
	11. SPONSOR/MONITOR'S REPORT NUMBER(S)

12. DISTRIBUTION/AVAILABILITY STATEMENT
Approved for public release; distribution unlimited

13. SUPPLEMENTARY NOTES

14. ABSTRACT

Near-ground aerosol fogs were applied in the Chihuahua Desert of New Mexico, which has widely spaced low shrub vegetation. Near-ground fog dispersion was measured remotely with a light detection and ranging (lidar) system. Local atmospheric turbulence and stability were continuously measured with 3-axis sonic anemometers during aerosol treatments. Lidar-measured plume area coverage and spread were related to the simultaneous local-scale weather including both convective boundary layers (CBL) and stable boundary layers (SBL). A modified bulk stability ratio (SRm) was used to characterize the stability conditions near the ground. Time averages appropriate to the SBL were determined using the multidimensional decomposition technique and matched to the short spray time periods in the CBL. The widest most effective, near-ground coverage was obtained from insect fogger applications conducted during relatively high wind speeds: U > 1 m s-1 in stable conditions, and U > 3 m s-1 in unstable conditions. In general, spraying during SBLs was more efficient than during CBLs, with less material wasted and better consistency of coverage in the target zone nearest the ground. There was no significant difference in spray coverage or plume dispersion between the handheld thermal fogger and the ultra-low volume (cold fogger) applicator used.

15. SUBJECT TERMS

16. SECURITY CLASSIFICATION OF:			17. LIMITATION OF ABSTRACT	18. NUMBER OF PAGES	19a. NAME OF RESPONSIBLE PERSON
a. REPORT	b. ABSTRACT	c. THIS PAGE			
unclassified	**unclassified**	**unclassified**	**Same as Report (SAR)**	**11**	

has also been used for monitoring other agriculture-related aerosols, e.g., the dispersion of smoke from forest fires (Lavrov et al., 2006) and mapping of spray drift from an air-carrier sprayer used in citrus applications during stable (nighttime) and unstable (daytime) meteorological conditions (Miller et al., 2003). Although lidar cannot provide aerosol concentrations directly and only scans above vegetation, Khot et al. (2011) have provided a method to use it to spatially extrapolate point sampler measurements above the vegetation.

The lidar studies mentioned above emphasized that atmospheric stability is one of the most important factors in determining spray dispersion of fine droplets across both space and time. These observations confirm the classical treatments of air pollution by Sutton (1947), Pasquill (1962), and others. The term "atmospheric stability" refers to the tendency of the atmosphere to generate or suppress turbulence in the airflow. Stull (1988), Garratt (1992), Arya (2001), and others have discussed the physics of boundary layer stability in considerable detail, including the effects on stability of each process in the turbulent kinetic energy (TKE) budget. In general, when the buoyancy force is upward, the air is unstable and turbulence is generated. When the buoyancy force is downward, the air is classified as stable because the negative heat flux acts to suppress turbulence.

The Monin-Obukhov (MO) stability parameter, ζ (Monin and Obukhov, 1954), which employs the ratio of buoyant and mechanical production processes, is often used to help classify the stability and turbulence conditions in the surface boundary layer. A limitation of this approach is that constant flux as a function of height is assumed, which is only valid in fully turbulent and horizontally homogeneous boundary layers. Thus, it is generally not valid in stable, low wind conditions. In the agricultural engineering spray literature, stability has been measured by the local vertical air temperature gradient divided by the square of wind speed. This parameter is termed the stability ratio (*SR*) after Munn (1966) and Yates et al. (1974). Fritz (2006) explained the ASABE standards inclusion of the stability ratio and its measurement. In this study, we employ a modification to this approach as a measure of stability in the desert conditions under investigation.

In the case of sporadic, ground-level sources (i.e., pesticide fog and spray), the aerosols are emitted only over short times and small areas. These sources therefore deposit or move out of the target area in only a few minutes. Thus, short-time local turbulent motions control the transport and deposition of the aerosol in the target area. These times and spaces are an order of magnitude smaller than the time averages of an hour or more used to include all the scales of turbulent motion in convective planetary boundary layers. But turbulence averaging times from seconds to a few minutes have been used in a number of studies of short-term event dispersion and emissions to characterize near-field dynamics such as dust emissions from tractor plowing (Holmen et al., 2008) and its transport modeling (Wang et al., 2008). Therefore, in the work reported here, we used short averaging times during the daytime to capture the turbulence and wind during the period directly influencing the spray movement over and in the target zone.

The study presented here focuses on the use of a ground-based, elastic backscatter lidar system and micrometeorology measurements near the ground for evaluating the dispersion of aerosol droplets in open-field applications. The objective of the study was to compare the movement of spray plumes from insect foggers and ULV applicators in various atmospheric stability conditions on time scales relevant to current application practices. This article also evaluates the effect of atmospheric surface layer conditions on the spray plume spread and the effective area coverage of drifting spray plumes in a desert environment.

MATERIAL AND METHODS

SPRAY EQUIPMENT AND APPLICATION

A field experiment was conducted at a small private airport near Las Cruces, New Mexico (32° 10' 33" N, 106° 46' 16" W). The experimental site included a paved runway at a slope of about 1.6° surrounded by sparse Chihuahua Desert vegetation approximately 2 m tall (fig. 1). The vegetation was primarily mesquite and creosote bushes that averaged about 1 m in diameter and were spaced irregularly, about 5 to 10 m apart on average, with the overall crown cover of less than 20%. Figure 2 shows an aerial view of the vegetation coverage on the site, including a portion of the runway. The extensive exposure of the desert ground surface limited the micrometeorology effects of the vegetation to primarily causing an increase in the surface roughness. No zero plane displacement of the wind profile was detected. Previous studies in the area (Wang et al., 2009; Zeweldi et al., 2010; and others) have shown that the very dry environment severely limited water vapor fluxes.

The experiments were conducted on September 9-17, 2008. In this article, we present results from trials using a handheld thermal fogger (T1) (Golden Eagle 2610, Curtis Dyna-Fog, Ltd., Westfield, Ind.) and a handheld ULV (cold fogger) applicator (U1) (Colt, London Fog, Inc., Long Lake, Minn.). The thermal fogger used a gasoline engine to disperse petroleum-based formulations by thermal atomization. The spray at the exit nozzle was 66.9°C with an exit velocity of 20.5 m s^{-1}. It was operated at a spray rate of 0.25 L min^{-1}. The ULV applicator used a two-cycle engine and air-shear nozzle to generate aerosol droplets at spray rate of 0.06 L min^{-1}. The spray at the exit nozzle was approximately 1.5°C higher than the ambient atmospheric temperature (~20°C) with an exit velocity of 12.8 m s^{-1}. Both sprayers were mounted on a custom-built trolley with an adjustable height platform. The trolley was pulled by a pickup truck at a nominal speed of 8 km h^{-1}. Each spray time replication (about 15 to 20 min duration) consisted of four spray runs, each about 90 s for a length of 200 m, on the runway. A total of 168 runs were made using both applicators during day and night. The spray mixture contained 5.29 mL L^{-1} of a fluorescent tracer (Uvitex TFR, Ciba-Geigy Corp., Greensboro, N.C.) dissolved in BVA-13 mineral oil (BVA, Inc., Wixom, Mich.).

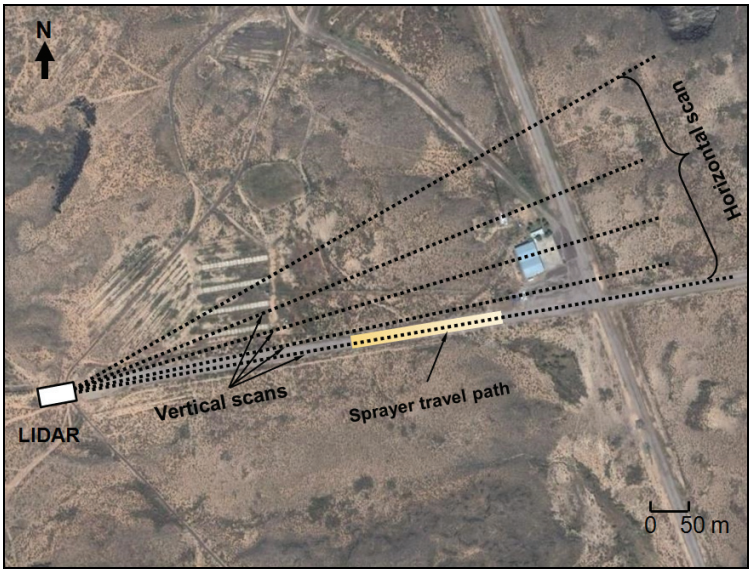

Figure 1. Aerial view of the test site and schematic of lidar scanning schemes.

Figure 2. Aerial view showing spacing of desert shrub vegetation and portion of runway used by sprayer vehicle.

The daytime runs were in unstable convective conditions, and the nighttime runs were generally in stable atmospheric conditions. Humidity was measured at 1 m height on the anemometer mast with a radiation-shielded temperature/RH probe (HMP-60, Campbell Scientific, Inc., Logan, Utah). Two 3-axis sonic anemometers (CSAT3, Campbell Scientific) were used to record three-component (u, v, w) wind velocities at a rate of 10 Hz during the spray applications. The sonic anemometers also measured sonic air temperature, which includes the effect of air humidity. Sonic air temperature is very nearly equivalent to virtual air temperature (Kaimal and Gaynor, 1991). Thus, the sonic air temperatures were used directly in the calculations reported here as the measure of virtual air temperature (θ_v). The anemometers were mounted at 1 m and 3 m above ground level about 2 m from the nearest bush. The specific humidity (q) measurements were used to estimate the difference between the dry air temperature and the sonic temperature after Schotanus et al. (1983). The dry air temperature (θ_a) averaged 1.05 K less than the sonic temperature and ranged from 0.53 K to 1.84 K less, as a function of q. An additional sensor (IR thermometer model R111, Apogee Instruments, Logan Utah, accuracy = 0.2°C, precision = 0.08°C) was used to measure radiant ground surface temperature (θ_g) between the widely spaced shrubs. It was mounted at 1 m height on the anemometer mast and pointed away and downward at a 60° angle to measure the surface temperature of a bare ground area approximately 4 m from the closest shrub. The sonic anemometer measurements were used to find the wind speed magnitude (U) and direction (U_{dir}) as well as heat flux (H), friction velocity (u^*), and the MO stability parameter (ζ) during each period of interest. The MO stability parameter is defined as:

$$\xi = \frac{z}{L} = \frac{-kzg < w'\theta_V' >}{\overline{\theta}_v u^{*3}} \quad (1)$$

where k is the von Karman constant (k = 0.4), z is the height above ground, g is the constant acceleration of gravity, L is the Monin-Obukhov length, and $<w'\theta_v'>$ is the vertical velocity to temperature covariance. An overbar indicates a time averaged value.

Two-minute time averages were used based on the multi-resolution decomposition calculation (Howell and Marht, 1997). This technique, applied to stable conditions, identified a spectral gap between 90 and 120 s. This technique is used to separate small turbulence fluxes from larger-scale non-turbulent motions. Thus, the 120 s averaging is a low-pass filter resulting in a time series affected only by local turbulence. During daytime CBL conditions, the spray could be detected over the target area for 5 to 10 min; therefore, the 2 min averages were also used in the daytime to record any trend during the spray dispersal and lidar scan periods. It also maintained consistency throughout all the trials in the calculation of stability, u^*, and H.

In this study, we modified the SR approach recommended in the literature (Fritz, 2006) to quantify the atmospheric stability. Due to the location of the upper sonic above the surrounding shrubs and the lower sonic between shrubs, the "homogeneous fetch" assumption necessary for the historic SR could not be made for the 1 m measurements at these short time averages. Therefore, we replaced the lower air temperature measurement (Fritz, 2006) with the radiant ground surface temperature (θ_g). The modified bulk stability ratio (SR_m) was more consistent and robust in this ground level environment and was a better indicator of the short time average heat flux, since the maximum temperature gradient was within the first few centimeters above the ground surface and could not be measured with the sonic anemometers:

$$SR_m = \frac{\theta_a - \theta_g}{U^2} \quad (2)$$

where θ_a is the air temperature at 3 m above ground, and θ_g is the ground surface temperature. Note that the use of the sonic temperature for θ_a results in an average 1.05 K positive bias in the measured dry air temperature. This added to the average ±0.2 K error in θ_g results in an estimated average gradient error (positive bias) of + 0.85 K to +1.25 K.

A modified stability ratio of 0.0 ±0.01 °C $(m/s)^{-2}$ indicates neutral conditions in the included air layer. In equation 2, an inverted temperature gradient (positive value) implies a stable condition, and a lapse temperature gradient (negative value) implies an unstable, convective condition. The wind speed in the denominator is the indicator of shear turbulence production. Figure 3 presents a time series of H from the sonic anemometer and SR_m. Note the close inverse correspondence between the heat flux and SR_m during the unstable hours. However, the correspondence during stable hours is subdued because SR_m is quite sensitive to fluctuations in the wind as well as the heat flux during stable hours. An example is the peak, indicating very intense stability, a few minutes after 21:00 h, when U and u^* dipped to near zero.

Droplet Size Characterization

Before the field experiments, spray droplet size distribution of the equipment was characterized using a 2-D phase Doppler particle analyzer (PDPA) system (TSI, Inc., Shoreview, Minn.). Droplet size measurements were made using BVA-13 mineral oil, without fluorescent tracer, as the spray solution, at distances of about 1.5 m from the sprayer outlet. For each applicator, measurements were replicated three times. For each replication, spray was released in the horizontal direction and was scanned vertically from top to bottom in a sweep (continuous) capture mode. Spray droplet size parameters, i.e., volume median diameter ($D_{v0.5}$) as well as 10% and 90% volume diameters ($D_{v0.1}$ and $D_{v0.9}$) of the generated aerosol are reported in table 1.

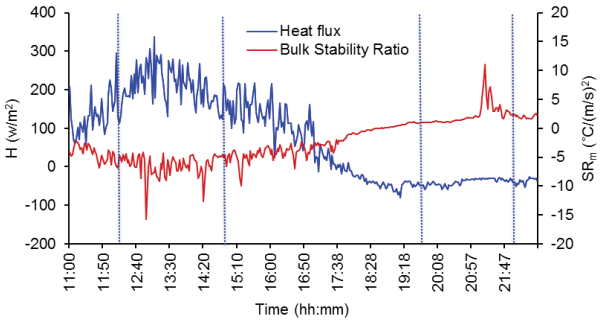

Figure 3. Trends of heat flux (H) and modified stability ratio (SR_m) with time. Vertical lines bracket the two periods (day and night, Sept. 16) of the spray trials.

Lidar Measurements

For each run, the truck started at 400 m from the lidar and moved along the runway for a total travel distance of 200 m (fig. 4). The University of Connecticut scanning elastic-backscatter lidar was used to scan the vertical and horizontal cross-sections of the spray plume, as shown in figure 1. Details of the lidar system can be found in Hiscox et al. (2006a), and the theory can be found in Kovalev and Eichinger (2004). The lidar uses a 1064 nm Nd:YAG transmitter and a 25 cm Cassegrain telescope to receive the backscattered signal. The system uses a silicon avalanche

Table 1. Droplet size data at 1.5 m from nozzle for the thermal fogger and ULV aerosol applicator.

Spray Equipment	Flow Rate (L min^{-1})	Droplet Size (µm, mean ±SD)		
		$D_{v0.1}$	$D_{v0.5}$	$D_{v0.9}$
Thermal fogger	0.18	2.0 ±0.2	4.9 ±1.1	20.6 ±3.9
ULV applicator	0.06	16.7 ±1.7	26.1 ±2.2	40.2 ±6.0

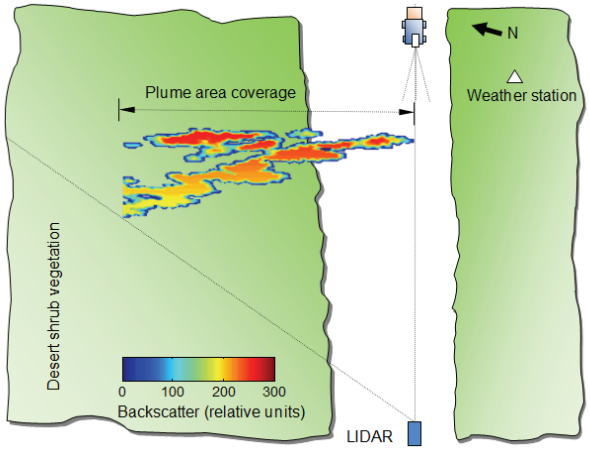

Figure 4. Schematic of the experiment showing the horizontal lidar scans.

photodetector to convert the light received to an electrical signal, which is then digitized by a Signatec PDA12 board (Signatec, Inc., Newport Beach, Cal.) and has a 1.55 m spatial resolution.

A different lidar scanning sequence was used for each of the four runs in the replication (runs 1 to 4). Spray application parameters and procedures were kept constant for each run. The first run (run 1) was intended to vertically scan the near-field plume cross-section by taking repetitive vertical slices at ~9 m and ~11 m downwind of the spray truck path. Run 2 was intended to scan the plume cross-section further downwind with repetitive slices at ~9 m, ~24 m, and ~32 m away from the spray truck path over the desert vegetation. The vertical extent of the scans was adjusted depending on field conditions and the height of the plume during the first run. Run 3 was intended to scan the plume horizontally using scans at increasing elevation angles. These were designed to scan a larger volume of the plume and ascertain the full extent of near-ground plume spread. During the final run (run 4), the lidar was used in a staring mode to record the velocity and variability of the plume near the spray truck. All lidar scans began ~30 s before the truck started to drive and continued until spray was no longer visible in the real-time display. This article reports on the far-field lidar vertical and horizontal scans data only (runs 2 and 3).

Plume Feature Extraction

Spray plume dispersion and movement were analyzed to determine the conditions that were likely to provide aerosol contact with flying insects. In this case, the effective area would be below the level of the shrub tops. It is assumed that the turbulence caused by the air moving across and through the bushes and over the ground mixes the air and spray vertically. Therefore, the lowest lidar horizontal scan in each replication, i.e., across the top of the canopy, was used to estimate the plume area coverage. The area was determined from the width (perpendicular to the spray travel path) and average length (along the spray travel path) of the coverage just above the shrub tops in an individual horizontal scan (fig. 4). The data were preprocessed using a program written in Interactive Data Language (IDL) software (ver. 7.1, ITT Visual Information Solutions, Boulder, Colo.). Standard lidar data correction procedures were followed for background subtraction and range-squared correction (Kovalev and Eichinger, 2004). The data were converted to an *xyz* Cartesian coordinate system with the lidar centered at the origin. Resulting arrays of data (x, y, z, and intensity) were then used to extract the plume features. A custom program was written in Matlab (ver. R2009a, The MathWorks, Inc. Natick, Mass.) to help the plume feature extraction process. The program also provided visualization of the spray plume. Examples of spray plume visualization are shown in figures 5 and 6.

Plume cross-sectional spread statistics can be used as the measure of dispersion of the plume perpendicular to the sprayer travel path, which is a major process determining the turbulence-driven reach and eventual dilution of the plume over time. Hiscox et al. (2010) showed that this process was responsible for only a minor portion of the plume dispersion in stable conditions, and plume meander driven by submesoscale winds was the primary process. In the unstable CBL, however, Hanna et al. (1982) and many others have shown that boundary layer turbulence is responsible for nearly all of the dispersion in the CBL where the turbulence scales are large enough to include plume meander. In this study, interest was in the comprehension of horizontal dispersion near the canopy top where the spray mixed up-and-down with that in the underlying layer of air containing the widely spaced shrubs. Vertical lidar scans across the plume were used to obtain the cross-sectional width at the bottom of the plume, i.e., the "connected" part of the plume just above the shrub tops. The plume width feature was extracted from vertical scans as the distance along the sprayer travel path with backscatter intensity above a threshold (within 300 to 700 m of the lidar). The intensity was a relative value with a useful threshold of 60 relative units, i.e., about 15% to 20% of the peak backscatter value in a given scan. The peaks were up to about 400 and 500 relative units for day and night lidar scans, respectively. The threshold was chosen after preliminary visual inspection of the scans. Total plume height estimates were not considered in this study because the plume often moved higher than lidar scan heights in high convection, low wind conditions, during daytime (figs. 5a and 6).

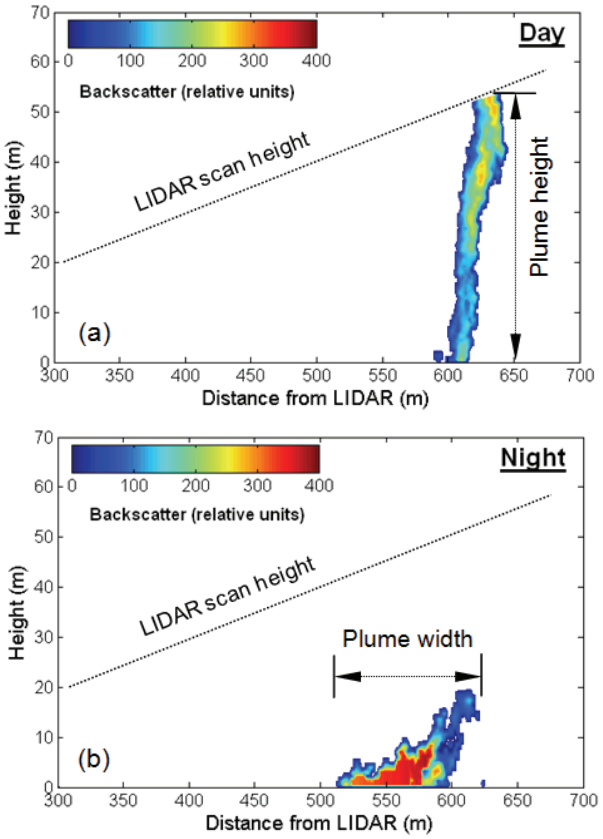

Figure 5. Typical vertical movement (run 2) of a spray plume from the handheld ULV applicator at 9 m downwind from the spray path: (a) daytime, (b) nighttime applications. The 0.0 height on the graph is the height of the lowest scan just above the tops of the shrubs (z = ~2 m).

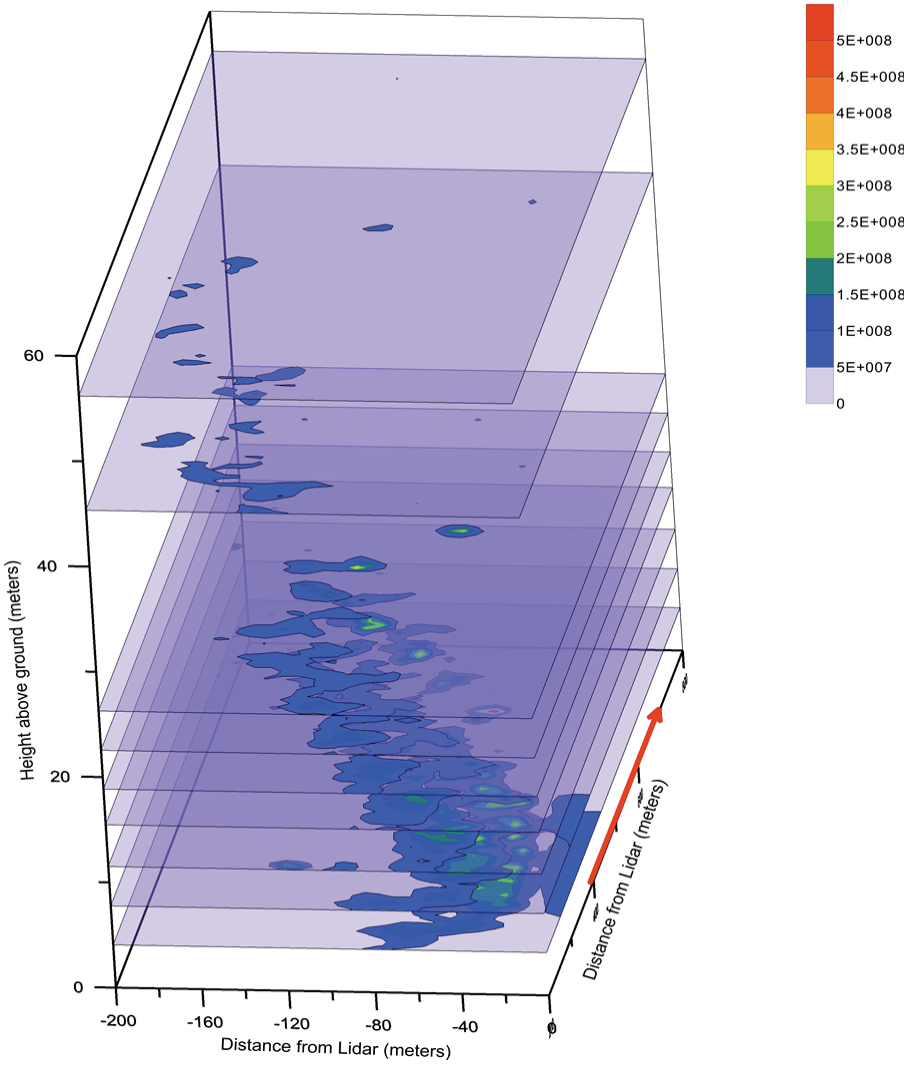

Figure 6. Oblique (facing east) view of lidar-measured spray cloud showing the separation of the fog from the ground/shrub layer and lofting into the atmosphere under CBL conditions at ~13:59 on September 15. The fog had been sprayed along the lower right edge of the graph.

The lidar could only scan above the brush and not through it. Therefore, no specific measurement of spray mixing downward to the ground surface below the scan location could be made. Previous work in closed canopies has indicated that mechanically generated turbulent eddies at the canopy top are intense enough to penetrate to the ground level during unstable periods. Kaimal and Finnigan (1994) provide a review and more recent work includes Aylor et al. (1993) in tall grass, Stoughton and Miller (2002) in hardwood forests, and Simmons et al. (2007) in pecan orchards, among others. In this sparse shrub desert environment, Nappo et al. (2010) showed that, during stable conditions, the flow at 11 m above the ground was decoupled from that at 1.5 m above the ground in low wind conditions. But at 1.5 m, there was always enough mechanical turbulence to ensure the formation of a ground-connected surface boundary layer, i.e., turbulence mixing the air down and up. Therefore, it was assumed that when spray was present just above the shrubs, as detected by the lidar, it mixed down to the ground level below that location.

Results

Weather During Aerosol Applications

Table 2 lists the 2 min averaged weather conditions during each sprayer pass. Daytime wind speeds ranged from 0.8 to 5.5 m s^{-1}, and the sensible heat flux (H) was generally high (100 to 200 W m^{-2}). Thus, the daytime atmospheric instability ranged from intensely unstable (SR_m = -16.8°C $(m/s)^{-2}$) to nearly neutral (SR_m = -0.5°C $(m/s)^{-2}$) at the higher wind speeds. The stability approached free convection on September 12 due to very low winds. It was near neutral on September 15 due to high winds (~5 m s^{-1}) and a high overcast, which resulted in a cooler ground surface. September 16 was moderately convective with moderate winds and partly cloudy sky.

Table 2. Weather parameters during horizontal lidar scans of spray runs.[a]

Time (hh:mm)	SR_m (°C (m/s)$^{-2}$)	U (m s^{-1})	H (W m^{-2})	U_{dir} (°)	θ_v (°C)	θ_g (°C)	RH (%)	Time (hh:mm)	SR_m (°C (m/s)$^{-2}$)	U (m s^{-1})	U_{dir} (°)	H (W m^{-2})	θ_v (°C)	θ_g (°C)	RH (%)
September 12															
Day								Night							
13:21	-11.8	1.5	236.1	253	25.0	42.0	35.7	21:19	0.1	2.1	140	27.0	22.4	21.9	62.5
15:01	-8.9	1.9	250.8	123	26.0	42.1	30.6	22:09	0.1	3.0	159	32.4	22.4	22.0	64.2
15:35	-13.1	1.4	173.2	250	26.5	42.7	27.3	22:43	0.0	2.5	251	38.5	21.8	21.8	67.8
16:16	-16.8	1.0	138.2	207	26.3	41.9	24.9	23:23	0.0	3.0	251	33.9	21.5	21.7	68.1
16:50	-9.0	0.8	63.7	159	25.8	33.0	38.7	23.53	0.1	2.4	246	30.6	21.4	21.6	69.5
								00:24	1.5	0.8	266	52.3	20.9	19.9	72.6
September 15															
Day								Night							
12:26	-1.0	4.0	139.3	253	21.5	37.4	25.1	20:08	0.2	2.7	205	43.5	18.1	19.4	60.1
13:19	-0.5	5.5	230.8	242	21.9	37.3	38.7	20:36	0.1	2.1	193	26.7	17.5	18.7	64.5
13:56	-0.9	4.0	297.4	230	22.5	37.5	38.1	21:04	0.0	1.9	195	36.2	16.9	16.9	68.4
14:30	-0.6	5.5	158.8	247	22.5	39.5	32.1	21:28	0.0	1.9	189	30.8	16.2	16.2	70.6
15:32	-0.6	5.1	217.6	220	22.5	37.4	29.6	21:53	0.1	1.4	179	42.5	15.9	15.7	69.3
15:59	-0.5	5.5	158.2	223	22.0	35.6	28.2	22:20	0.1	1.3	182	25.5	15.4	15.2	71.6
September 16															
Day								Night							
12:23	-5.4	3.4	203.5	67	22.2	40.6	26.3	19:54	1.2	1.5	340	-39.5	20.5	18.9	39.9
12:49	-15.8	1.5	218.3	61	22.2	42.7	25.6	20:20	1.0	2.1	336	-52.7	20.3	18.3	37.3
13:20	-5.4	4.0	219.5	41	23.4	44.6	23.5	20:57	2.2	0.7	6	-31.6	18.7	17.3	45.0
13:55	-4.8	4.3	201.8	43	24.4	44.6	22.1	21:25	2.9	1.3	325	-34.6	17.9	16.2	59.5
14:21	-5.4	3.9	154.9	54	24.1	44.2	21.5	21:47	2.8	0.9	352	-33.9	18.4	15.8	60.8
14:46	-4.6	4.2	133.4	24	24.5	42.4	24.4	22:09	2.3	0.9	20	-33.0	17.9	15.9	53.1
September 17								Transition							
								18:22	-0.4	2.5	134	2.5	24.7	25.7	
								18:48	0.1	2.0	143	-18.7	22.6	23.4	
								19:12	0.7	1.6	29	-19.7	22.7	22.7	
								19:25	0.9	1.4	298	-15.3	22.3	22.0	
								20:07	1.06	1.9	210	-21.4	21.3	19.3	
								20:36	1.48	1.5	305	-21.1	20.8	18.6	

[a] SR_m, U, U_{dir}, H, θ_v, θ_g, and RH are 2 min averages of modified stability ratio (eq. 2), wind speed, wind direction, surface sensible heat flux, air temperature at 3 m height, ground surface temperature, and relative humidity, respectively.

Wind speeds at night ranged from 3.0 m s^{-1} down to 0.7 m s^{-1}. This resulted in nighttime stabilities ranging from neutral (SR = 0.0°C (m/s)$^{-2}$) during the highest wind speeds to moderately stable (SR = +2.9°C (m/s)$^{-2}$). September 12 was near neutral during most of the runs due to high winds (U > 2 m^{-1}). September 15 was near neutral due to moderate winds and a high, thin overcast moderating the temperature difference between the ground surface and air. September 16 was intensely stable with very low winds. The transition period on September 17 changed from slightly unstable to moderately stable with light winds.

Ground surface temperature ranged from daytime highs approaching 45°C to nighttime lows near 15°C. Air temperatures ranged from a daytime high of 26.5°C to a nighttime low of 15.4°C. Relative humidity ranged from a daytime low of 21.5% to a nighttime high of 72.6%. These conditions were within the local, long-term ranges reported for September, which have ranged from 14°C to 30°C, with daytime relative humidity averaging 28%.

In stable conditions, the heat flux measured above the sparse brush indicated weak upward buoyancy on September 12 and 15, nights that were nearly neutral during the spray periods. But near the ground, the presence of a ground surface inversion (positive SR_m) indicated a downward flux of heat near the ground surface. This divergence of heat flux was likely due to advection above the shrub layer in weak cold air drainage on the east aspect, lightly sloping terrain. The day/night transition period on September 17 was unexpectedly stable, as shown by the mostly positive values of SR_m. Since the land sloped slightly to the east, the sun had stopped heating the ground and the ground surface rapidly cooled by radiant heat loss to the clear sky. Therefore, the runs during the transition period were lumped into the stable boundary layer category in the following analyses.

PLUME AREA COVERAGE AND SPREAD

The lidar volume scans were used to indicate the "connectedness" of the spray cloud above the tops of the shrubs to spray mixing down to the ground surface, as explained above. Figure 6 shows an example on September 16. It shows lidar-measured plumes from a single pass of the fogger during a CBL. Note that the fog cloud (U = ~4 m s^{-1}) has spread out from the sprayer path along the right bottom edge of the bounding box, but it is separating from the surface and rising into the air. The area within 50 m of the spray path contains the lowest portion of the plume near the ground. This area was interpreted as the "connected" area. The area under the portion of the plume lifting off the surface was interpreted as the "not connected" area. Note also that the fog cloud is not continuous along the sprayer path, even though the spray application was continuous. Apparently, the fog has been organized into several elongated plumes, which are rising in the air with some residual fog near the ground below each of them. It is likely that these plumes were separated by classic surface layer thermal eddy structures that move along the ground during ful-

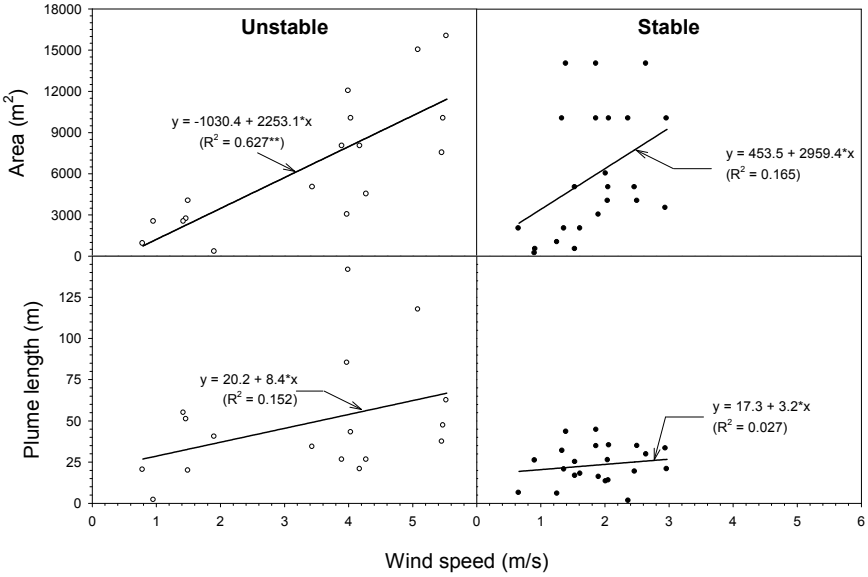

Figure 7. Plume coverage area and cross-sectional length during unstable (daytime) and stable (nighttime) atmosphere conditions as the function of wind speed.

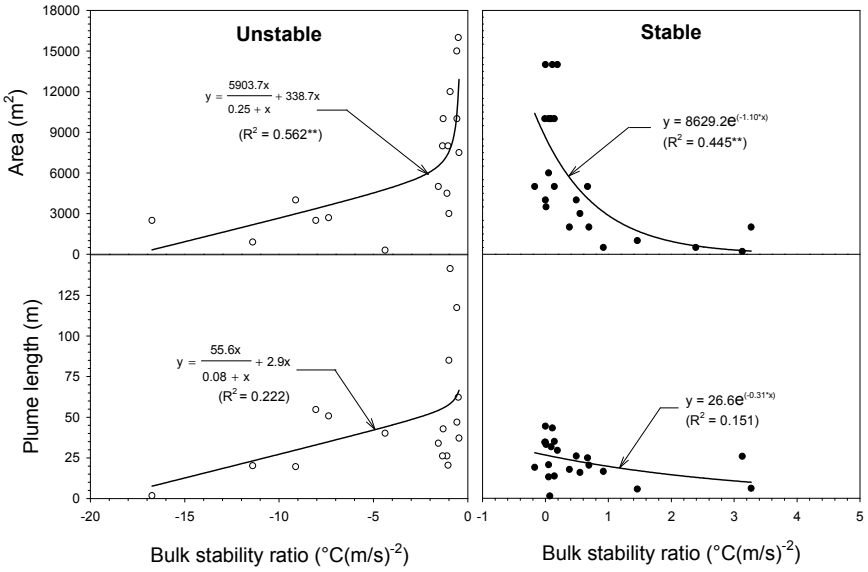

Figure 8. Plume coverage area and cross-sectional length during unstable (daytime) and stable (nighttime) atmosphere conditions as a function of SR_m.

ly developed CBLs. In this case, the spatial scale of both height and separation is on the order of 70 m.

Relatively strong unstable, upward buoyancy during the day time, driven by upward surface sensible heat flux, resulted in rapid rise of spray in convective plumes, as shown in figure 5a, whenever the wind speed was low (i.e., below ~2.0 m s^{-1}). Therefore, although it was originally connected, the spray covered a minimum area, only about 10 m across the plume (fig. 5a). Convection cells moved it upward from the ground surface rather quickly in low wind conditions. This pattern was broken up during higher wind conditions when the cloud spread both horizontally and vertically, as shown in figure 6.

Figure 7 presents the relationship between plume area coverage and wind speed for all trials during unstable and stable atmospheric conditions. In general, the horizontal coverage area is widely scattered but increases with wind during unstable atmospheric conditions. Similar trends were observed during stable conditions as well, but with lower wind. Figure 7 also shows the plume cross-sectional widths, measured at about 32 m distance from the sprayer path. In unstable conditions, it appears that the plume cross-sectional width increases with higher winds, similar to the area coverage above, but the scatter is extreme. During stable conditions, the plume widths (fig. 7) showed essentially no response to wind speed. In the unstable boundary layer, the higher wind speeds generated more mechanical turbulence across the top of the brush, which resulted in higher plume cross-sectional width.

Figure 8 shows the area coverage and plume cross-sectional width as functions of the modified bulk stability ratio. There is low area coverage at high convection intensi-

ties (i.e., large negative SR_m), and coverage increases in a highly non-linear manner as convection intensity is broken down by higher wind speeds. During nighttime applications, wind speeds above 1 m s^{-1} cause near-neutral stable conditions and result in the larger area coverage. Additionally, the exponential relationship between the intensity of the surface inversion, indicated by the positive increase in SR_m, and the plume cross-sectional width can be seen. A steep, non-linear increase in plume cross-sectional width and area coverage occurred near neutral ($0 < SR_m < -1$), where higher winds broke up the strong heat convection. It appears that this happened at about 4 m s^{-1}.

DISCUSSION

The thermal fogger produced the smallest droplets ($D_{v0.5}$ = ~5 µm, settling velocity = ~7.8 × 10^{-5} m s^{-1}) compared to the ULV applicator ($D_{v0.5}$ = ~26 µm, settling velocity = ~0.072 m s^{-1}). The variations in weather conditions were dominant over any differences in the applicators during the field experiments. We would like to note that it is expected that variation in droplet size and therefore settling velocity would play a role in the total ground deposition of spray. Under the conditions of these trials, however, no such contribution was observed. This can simply be attributed to the fact that the downward motion due to settling would occur on a longer time scale than the lidar visualizations can detect.

Considerable work on downward eddy gusts and upward air ejections near the ground and in vegetation has demonstrated dispersion downward to the ground surface, even under complete canopies (Baldocchi and Meyers, 1998; Kaimal and Finnigan, 1994). The assumption that these processes ensured vertical connection to the ground surface in this environment was checked by comparing time series of the instantaneous wind components from the anemometers at 3 and 1 m. These comparisons (not shown) clearly showed that the assumption was true in the daytime convective boundary layer and in the nighttime stable layer with some wind. But the results were less clear in the very calm stable periods.

The obvious differences between unstable (daytime) and stable (nighttime and evening transition) periods were the different wind regimes and the direction and intensities of the surface heat fluxes. A greater range of wind with generally higher speeds in the unstable periods and heat fluxes that were an order of magnitude higher and in different directions than during stable conditions resulted in strikingly different vertical movements of the spray plumes. Daytime conditions fell into two general regimes: those with winds <3 m s^{-1}, and those with winds generally >3 m s^{-1}. These are typified by the graphs in figures 5a and 6, respectively. The spray clouds in low winds (i.e., fig. 5a) contained very little spray at lower levels, with most of the spray rising vertically into the boundary layer. In higher winds, the spray spread horizontally, but a significant amount rose well above the surface and was removed from the target area. For example, figure 6 shows most of the spray material in the air well above the level of the shrub tops, whereas figure 5b shows that all of the spray material was within 15 m of the ground surface during stable conditions.

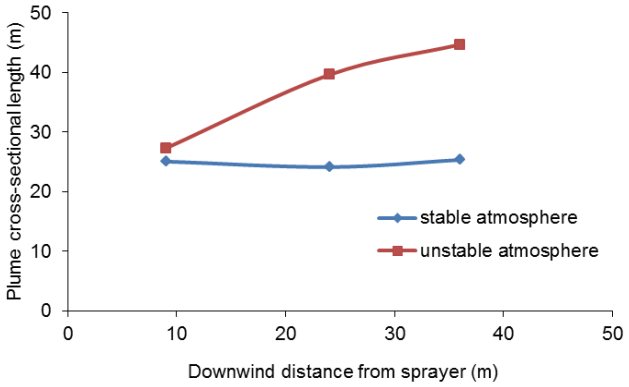

Figure 9. Average plume spread with downwind distance from the sprayer travel path during stable (night) and unstable (day) periods.

The average cumulative effect on plume spread, as measured by cross-sectional width, is not as dramatic. The widths, averaged across all the plumes, are shown in figure 9. The variability of the cross-sectional widths during CBLs were higher, as measured by the coefficients of variation (CV = standard deviation/mean) of the measured plume widths at each of the downwind cross-sectional scan locations. The CV values averaged 70% during the CBL and 56% during the SBL. The unstable daytime atmosphere resulted in wider spreading, but more variable, plumes as they moved downwind. When stable, the plume widths were essentially unchanged downwind. The cross-sectional plume spread during unstable conditions was smaller but otherwise generally in agreement with estimates using Gaussian plume spread equations. During stable conditions, the lack of any widening of the plume was somewhat unexpected where traditional descriptions suggest "fanning" should take place. We attribute these disagreements to the instantaneous nature of the individual lidar measurements, which do not accumulate the turbulent meander motions included in the longer-time averaged parameterizations of the classic Gaussian plume equations.

CONCLUSIONS

- The widest, most effective, near-ground coverage was obtained from insect fogger applications conducted during relatively high wind speeds: U > 1 m s^{-1} in stable conditions, and U > 3 m s^{-1} in unstable conditions. The highest winds forced the stability toward neutral during these periods. Spraying during periods with more intense convection, i.e., wind speeds <3 m s^{-1} in unstable periods, resulted in less consistent coverage, with most of the spray material quickly lifting out of the target zone in convection plumes. Intense SBLs, with winds <1 m s^{-1}, resulted in the formation of weak, intermittent cold air drainage moving some portions of the spray down the shallow slope.
- In general, spraying during SBLs was more efficient than during CBLs, with less material wasted and bet-

ter consistency of coverage in the target zone nearest the ground.

- Even with the relatively high wind conditions, most of the sprayed material during CBL conditions was in the air well above the surface roughness elements. Therefore, it is likely that higher volumes of spray would result in better efficacy in CBLs since a large percentage is rapidly lost.
- There was not a marked difference in spray coverage or plume dispersion between the handheld thermal fogger and ULV applicator in the short time periods when the spray was moving in the target area. Both produced "light" particles that were readily lifted by convection or advected by the local wind.

ACKNOWLEDGEMENTS

This study was partially supported by a grant from the U.S. Armed Forces Pest Management Board, Deployed War-Fighter Protection (AFPMB/DWFP) research program. Support was also received from the University of Florida IFAS, University of Connecticut, Storrs Agricultural Experiment Station, U.S. Navy Entomology Center of Excellence, and the New Mexico State University Agricultural Experiment Station. The authors acknowledge technical assistances of Roy Sweeb (UF/IFAS), Vincent Smith and Cathy Robinson (NECE), Junming Wang and Mark Pacheco (NMSU), and David Ganucci (UConn).

REFERENCES

Aronson, N. E. 2007. Leishmaniasis in American soldiers: Parasites from the front. In *Emerging Infections* 7: 346-364. W. M. Scheld, D. C. Hooper, and J. M. Hughes, eds. Washington, D.C.: ASM Press.

Arya, S. P. 2001. *Introduction to Micrometeorology*. 2nd ed. San Diego, Cal.: Academic Press.

Aylor, D. E., Y. Wang, and D. R. Miller. 1993. Intermittent wind close to the ground within a grass canopy. *Boundary Layer Meteorol.* 66(4): 427-448.

Baldocchi, D. D., and T. P. Meyers. 1998. On using eco-physiological, micrometeorological, and biogeochemical theory to evaluate carbon dioxide, water vapor, and gaseous deposition fluxes over vegetation: A perspective. *Agric. Forest Meteorol.* 90(1-2): 1-26.

Barber, J., M. Greer, and A. Hewitt. 2004. A field measurement device for the aerosols used in mosquito control. ASAE Paper No. AA040010. St. Joseph, Mich.: ASAE.

Bonds, J. A., M. J. Greer, B. K. Fritz, and W. C. Hoffmann. 2009. Aerosol sampling: Comparison of two rotating impactors for field droplet sizing and volumetric measurements. *J. American Mosquito Control* 25(4): 474-479.

Collins, R. T. H. 1968. Lidar observations of atmospheric motion in forest valleys. *Bull. American Meteorol. Soc.* 49(9): 918-922.

Farooq, M., W. C. Hoffmann, T. W. Walker, V. L. Smith, C.A. Robinson, J. C. Dunford, and I. W. Sutherland. 2009. Samplers for evaluation and quantification of ultra-low volume space sprays. *J. American Mosquito Control* 25(4): 521-524.

Fritz, B. K. 2006. Meteorological effects on deposition and drift of aerially applied sprays. *Trans. ASABE* 49(5): 1295-1301.

Garratt, J. R. 1992. *The Atmospheric Boundary Layer*. Cambridge, U.K.: Cambridge University Press.

Hanna, S. R., G. A. Briggs, and R. P. Hosker. 1982. *Handbook on Atmospheric Diffusion*. Washington, D.C.: U.S. Department of Energy, Office of Energy Research.

Hiscox, A. L., C. J. Nappo, and D. R. Miller. 2006a. On the use of lidar images of smoke plumes to measure dispersion parameters in the stable boundary layer. *J. Atmos. Oceanic Tech.* 23(8): 1150-1154.

Hiscox, A. L., D. R. Miller, C. J. Nappo, and J. Ross. 2006b. Dispersion of fine spray from aerial applications in stable atmospheric conditions. *Trans. ASABE* 49(5): 1513-1520.

Hiscox, A. L., D. R. Miller, and C. J. Nappo. 2010. Plume meander and dispersion in a stable boundary layer. *J. Geophysical Res.* 115: D21105.

Hoff, R. M., R. E Mickle, and F. A. Froude. 1989. A rapid acquisition lidar system for aerial spray diagnostics. *Trans. ASAE* 32(5): 1522-1528.

Holmen, B. A., D. R. Miller, A. L. Hiscox, W. Yang, J. Wang, T. Sammis, and R. Bottoms. 2008. Near-source particulate emissions and plume dynamics from agricultural field operations. *J. Atmos. Chem.* 59(2): 117-134.

Howell, J. F., and L. Mahrt. 1997. Multiresolution flux decomposition. *Boundary Layer Meteorol*. 83(1): 117-137.

Kaimal, J. C., and J. J. Finnigan. 1994. *Atmospheric Boundary Layer Flows*. New York, N.Y.: Oxford University Press.

Kaimal, J. C., and J. E. Gaynor. 1991. Another look at sonic thermometry. *Boundary Layer Meteorol*. 56(4): 401-410.

Khot, L. R., D. R. Miller, A. L. Hiscox, M. Salyani, T. W. Walker, and M. Farooq. 2011. Extrapolation of droplet catch measurements in aerosol application treatments. *Atomization and Sprays* 21(2): 149-158.

Kovalev, V. A., and W. E. Eichinger. 2004. *Elastic Lidar Theory, Practice, and Analysis Methods*. Hoboken, N.J.: John Wiley and Sons.

Lavrov, A., A. B. Utkin, R. Vilar, and A. Fernandes. 2006. Evaluation of smoke dispersion from forest fire plumes using lidar experiments and modeling. *Intl. J. Thermal Sci.* 45(9): 848-859.

McFee, R. B. 2008. Gulf war servicemen and servicewomen: The long road home and the role of health care professionals to enhance the troops' health and healing. *Disease-a-Month* 54(5): 265-333.

Mickle, R. E. 1994. Utilizing vortex behavior to minimize drift. *J. Environ. Sci. Health B* 29(4): 621-645.

Miller, D. R., M. Salyani, and A. Hiscox. 2003. Remote measurement of spray drift from orchard sprayers using lidar. ASAE Paper No. 031093. St. Joseph, Mich.: ASAE.

Monin, A. S., and A. M. Obukhov. 1954. Basic laws of turbulent mixing in the ground layer of the atmosphere. *Tr. Akad. Nauk SSSR Geofiz. Inst.* 24(151): 163-187. Translated from Russian. Available at: http://tss.asminternational.org.

Munn, R. E. 1966. *Descriptive Micrometeorology*. Advances in Geophysics 1. New York, N.Y.: Academic Press.

Nappo, C., A. Hiscox, and D. Miller. 2010. A note on turbulence stationarity and wind persistence with the stable planetary boundary layer. *Boundary Layer Meteorol*. 136(1): 165-174.

Nuyttens, D., M. De Schampheleire, P. Verboven, and B. Sonck. 2009. Comparison between indirect and direct spray drift assessment methods. *Biosyst. Eng.* 105(1): 2-12.

Pages, F., M. Faulde, E. Orlandi-Pradines, and P. Parola. 2010. The past and present threat of vector-borne diseases in deployed troops. *Clin. Microbiol. Infec.* 16(3): 209-224.

Pasquill, F. 1962. *Atmospheric Dispersion.* London, U.K.: D. Van Nostrand.

Salyani, M., and R. P. Cromwell. 1992. Spray drift from ground and aerial applications. *Trans. ASAE* 35(4): 1113-1120.

Schleier, J. J. III, and R. K. D. Peterson. 2010. Deposition and air

concentrations of permethrin and naled used for adult mosquito management. *Arch. Environ. Contam. Toxicol*. 58(1): 105-111.

Schotanus, P., F. T. M. Nieuwstadt, and H. A. R. DeBruin. 1983. Temperature measurement with a sonic anemometer and its application to heat and moisture fluctuations. *Boundary Layer Meteorol.* 26(1): 81-93.

Simmons, L. J., J. Wang, T. W. Sammis, and D. R. Miller. 2007. An evaluation of two inexpensive energy-balance techniques for measuring water use in flood-irrigated pecans (*Carya illinoinensis*). *Agric. Water Mgmt.* 88(1-3): 181-191.

Solanelles, F., E. Gregorio, R. Sanz, J. R. Rosell, J. Arnó, S. Planas, A. Escolà, J. Masip, M. Ribes-Dasi, F. Gracià, and F. Camp. 2009. Spray drift measurements in tree crops using a lidar system. In *Book of Abstracts: 10th Workshop on Spray Application Techniques in Fruit Growing*, 40-41. Wageningen, the Netherlands: Wageningen UR.

Stoughton, T. E., and D. R. Miller. 2002. Vertical dispersion in the nocturnal, stable surface layer above a forest canopy. *Atmos. Environ.* 36(24): 3989-3997.

Stoughton, T. E., D. R. Miller, X. Yang, and K. M. Ducharme. 1997. A comparison of spray drift predictions to lidar data. *Agric. Forest Meteorol.* 88(1-4): 15-26.

Stull, R. B. 1988. *An Introduction to Boundary Layer Meteorology*. Boston, Mass.: Kluwer Academic.

Sutton, O. G. 1947. The theoretical distribution of airborne pollution from factory chimneys. *Qtly. J. Royal Meteorol. Soc.* 73(317-318): 426-436.

USACHPPM. 2005. Diagnosis and treatment of diseases of tactical importance to U.S. central command. Technical Guide 273. Aberdeen Proving Ground, Md.: U.S. Army Center for Health Promotion and Preventive Medicine. Available at: http://handle.dtic.mil/100.2/ADA457189. Accessed 19 November 2010.

Wang, J., A. L. Hiscox, D. R. Miller, T. H. Meyer, and T. W. Sammis. 2008. A dynamic Lagrangian, field-scale model of dust dispersion from agriculture tilling operations. *Trans. ASABE* 51(5): 1763-1774.

Wang, J., T. W. Sammis, V. P. Gutschick, M. Gebremichael, and D. R. Miller. 2009. Sensitivity analysis of the surface energy balance algorithm for land (SEBAL). *Trans. ASABE* 52(3): 801-811.

Yates, W. E., N. B. Akesson, and R. E. Cowden. 1974. Criteria for minimizing drift residues on crops downwind from aerial applications. *Trans. ASAE* 17(4): 637-632.

Zeweldi, D. A., M. Gebremichael, J. Wang, T. Sammis, J. Kleissl, and D. R. Miller. 2010. Intercomparison of sensible eat flux from large-aperture scintillometer and eddy covariance methods: Field experiment over a homogeneous semi-arid region. *Boundary Layer Meteorol.* 135(1): 151-159.